European Journal of Pharmaceutical Sciences 223 (2026) 107562

Contents lists available at ScienceDirect

European Journal of Pharmaceutical Sciences

journal homepage: www.elsevier.com/locate/ejps

Preformulation studies of levonorgestrel: A supplier variation analysis

Clarice Sombra de Medeiros [a], Magnus Ipsen Pedersen [a], Mathias Dam Mønster Sørensen [a], Chloe Hopper [a], Martin Aage Barsøe Hedegaard [b], Sheng Qi [c], Zahari Vinarov [d,e], René Holm [a,*]

[a] University of Southern Denmark, Department of Physics, Chemistry and Pharmacy, Campusvej 55 5230, Odense, Denmark
[b] University of Southern Denmark, Department of Green Technology, Campusvej 55 5230, Odense, Denmark
[c] University of Liverpool, School of Pharmacy and Pharmaceutical Sciences L69 3GE, Liverpool, United Kingdom
[d] University of Sofia, Department of Chemical and Pharmaceutical Engineering, Marin Rusev Street 4 1164, Sofia, Bulgaria
[e] BIORESOURCES BG, Ruski blvd. 139 4000, Plovdiv, Bulgaria

ARTICLE INFO

Keywords:
Levonorgestrel
Preformulation
Characterization
Solubility

ABSTRACT

Levonorgestrel (LNG) is a second-generation synthetic progestogen that has been widely used in oral tablets for emergency contraception, intrauterine devices and transdermal implants. The main objectives of the present work were to evaluate LNG drug substance variability with respect to polymorphism and purity, and to investigate the stability of the compound in the selected organic solvents, pharmaceutical vehicles and biorelevant media. Solid-state analysis of LNG samples from eleven different suppliers were conducted by different analytical techniques, including Fourier transform infrared (FTIR), Raman, solid-state and liquid-state nuclear magnetic resonance (NMR) spectroscopies, differential scanning calorimetry (DSC), thermogravimetric analysis (TGA), powder X-ray diffraction (XRPD), wide-angle X-ray scattering (WAXS), small-angle X-ray scattering (SAXS) and scanning electron microscopy (SEM). In addition, dynamic vapour sorption (DVS) was performed to investigate the hygroscopicity of LNG. The comprehensive solid-state investigation of LNG from different sources showed only minor variations related to their thermal properties. Overall, all suppliers delivered the same polymorphic form of LNG and the compound displayed high physical stability under elevated temperatures and across relevant organic solvents, suggesting limited risks associated with polymorphic changes during processing. Moreover, the equilibrium solubility was obtained in a wide range of relevant organic solvents, dissolution media and pharmaceutical vehicles, which would support development of new dosage forms containing LNG.

1. Introduction

Unintended or unplanned pregnancy has a significant impact on the social and economic conditions of families worldwide. Moreover, the use of birth control has contributed to the improvement in maternal health and reduction of infant mortality (Frost and Lindberg, 2013; Gipson et al., 2008). Some of the modern contraceptive methods include oral contraceptive tablets, rod-shaped implants, intra-uterine devices (IUD), subcutaneous injections and intravaginal rings (WHO, 2023). Nevertheless, a recent study has estimated that, among the unintended pregnancies reported worldwide, the sub-Saharan Africa displayed the highest annual averages per 1000 women aged 15–49 years, although large regional and country differences have been reported (Bearak et al., 2022). For example, Bearak and co-workers reported 49 in Niger, 145 in Uganda and 35 in Europe and Northern America (Bearak et al., 2022). Low contraceptive adherence in sub-Saharan populations may be due to limited access to safe and effective contraceptive options that enable self-administration and are easily accepted by patients, particularly in regions with less access to health care providers (Li et al., 2022). A recent study reported that the most used family planning method across most countries in sub-Saharan Africa are injectable contraceptive formulations (39.4%), including intramuscular (e.g. Depo-Provera®) or subcutaneously administered formulations (Boadu, 2022; Jain et al., 2004). However, as administration of an injection often involves contact with a health care professional, geographic and social barriers may limit the use of family planning services in the sub-Saharan region (Ayuk et al., 2022). Therefore, the development of alternative contraceptive methods that are safe and easily self-administered, such as subcutaneous injections or transdermal patches (e.g. microneedles or microarray patches) could be highly relevant for this particular region (Li et al., 2022).

Norgestrel was first synthesized in the 1950s as a racemic mixture,

* Corresponding author at: Department of Physics, Chemistry and Pharmacy, University of Southern Denmark, Campusvej 55 5230, Odense, Denmark.
E-mail address: reho@sdu.dk (R. Holm).

https://doi.org/10.1016/j.ejps.2026.107562
Received 22 November 2025; Received in revised form 21 April 2026; Accepted 19 May 2026
Available online 22 May 2026

where levonorgestrel (LNG) (see Fig. 1) is the biologically active enantiomer, previously known as d-norgestrel (Kook et al., 2002). LNG is a well-known synthetic progestogen that has been used in oral tablets for emergency contraception (e.g. Plan B® pills) as well as in long-acting contraceptive methods, such as intrauterine devices (e.g. Mirena® and Liletta®) and subdermal implants (e.g. Norplant® and Jadelle®) (Fanse et al., 2022), hence it's a well-known effective and safe compound for contraception. The contraceptive efficacy of LNG is based on several mechanisms of actions that include ovulation inhibition, decreased cervical mucus permeability, fallopian tube motility, and endometrial receptivity (Duijkers et al., 2022).

LNG has three reported polymorphs: α, β and γ, of which α and β have been identified as the metastable forms and γ the stable form (Cao et al., 2017). The α form has been reported to display the fastest dissolution rate and the γ form the slowest (Cao et al., 2017). To the best of our knowledge, no comparative studies have evaluated the bioavailability or clinical efficacy when administering different polymorphic forms of LNG. For doses below 30 μg, a BSC-based biowaiver is permitted according to WHO guidance (WHO, 2026), whereas at higher doses the γ form may display lower bioavailability than the α form (Cao et al., 2017).

Stability studies support formulation development and excipient selection, as well as the determination of the optimal manufacturing method, shelf life, and storage conditions for drug products (Rehman et al., 2020). In a recent isoconversional study of LNG, Ridichie and coworkers (2023), investigated the thermolysis mechanism of LNG by using kinetic analysis to explore how LNG decomposes under oxidative conditions at elevated temperatures. The results suggested that LNG has complex decomposition mechanisms and that specific excipients might display a stabilizing effect on the decomposition of LNG (Ridichie et al., 2023). Another study conducted by Ridichie et al. (2024) investigated the compatibility between LNG and different pharmaceutical excipients in physical binary mixtures applying thermal analysis, infrared spectroscopy, and powder X-ray diffraction (XRPD). The results showed that only five excipients (i.e. microcrystalline cellulose, sodium carboxymethyl cellulose, calcium lactate pentahydrate, α-lactose monohydrate, and talc) did not display chemical interactions with LNG at room temperature or when heated (Ridichie et al., 2024). Bao and colleagues investigated the impact of curing conditions on the physical and chemical stability of LNG loaded into polydimethylsiloxane (PDMS)-based intrauterine devices and reported that the crystalline form of LNG was maintained inside the PDMS matrix and that the chemical stability of the API was not affected despite of a high processing temperature of 80 °C (Bao et al., 2018). Similar to intrauterine devices, other formulations such as microneedle patches also incorporate LNG in the solid state. Therefore, key solid-state properties, including particle size, morphology, and degree of crystallinity, may be critical material attributes that must be characterized during the development of novel LNG formulations (Fanse et al., 2022). In this context, preformulation studies are of great importance to ensure informed decision-making during the drug formulation stage and to increase manufacturing robustness. Furthermore, material variability in the provided active ingredient may be a critical factor to consider during the drug formulation stage (Stauffer et al., 2018). The influence of variability would be a natural part of a regulatory file, however, such investigations are rarely available in the public domain. Provided that novel formulations containing LNG may have a considerable impact in a Global public health context, the main objectives of the present work were to evaluate LNG drug substance variability with respect to polymorphism and purity, to investigate the polymorphic stability of the compound, and to determine the solubilities in the selected organic solvents, pharmaceutical vehicles and biorelevant media to support formulation developers. The analytical methods that were employed included thermal analysis (TGA/DSC), Attenuated Total Reflection Fourier Transform Infrared spectroscopy (ATR-FTIR), Raman spectroscopy, scanning electron microscopy (SEM), XRPD, WAXS, SAXS, laser diffraction through wet dispersion, dynamic vapor sorption (DVS) and solid-state and liquid-state nuclear magnetic resonance (NMR) spectroscopy.

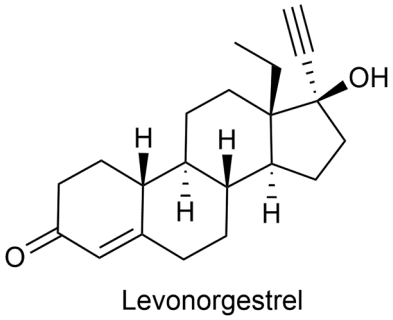

Fig. 1. Chemical structure of levonorgestrel.

2. Materials and methods

2.1. Materials

LNG was obtained from 11 different sources. The reported purities on the certificate of analysis and batch numbers are listed in Table 1.

The solvents investigated were obtained from different sources. N-methyl-2-pyrrolidone (NMP) 99.5% and ethyl acetate 99% were obtained from Thermo Scientific (Waltham, MA, USA); dimethyl sulfoxide (DMSO) 99.9% from Thermo Scientific (Waltham, MA, USA); deuterated DMSO from Sigma-Aldrich (Burlington, MA, USA); 1,4-dioxane from Sigma-Aldrich (Hamburg, Germany); diethylene glycol dimethyl ether (Diglyme) anhydrous 99,5% from Sigma-Aldrich (Burlington, MA, USA); tetrahydrofuran (THF) from VWR (Gdansk, Poland); dimethylformamide (DMF) from VWR (Darmstadt, Germany); dichloromethane (DCM) from VWR (Fontenay-sous-Bois, France) isopropanol and acetonitrile were obtained from VWR (Radnor, PA, USA); N,N-dimethylacetamide 99% (DMA) was purchased from Acros Organics (Geel, Belgium); acetone and ethanol 96% from VWR (Paris, France); methanol from VWR (Oslo, Norway) and toluene from Sigma-Aldrich (St. Louis, MO, USA).

The pharmaceutical excipients and other compounds used were Polysorbate 80 (PS80) and Polysorbate 20 (PS20) from Sigma-Aldrich (St. Louis, MO, USA); Poloxamer 188 from Thermo Scientific (Kandel, Germany); Kolliphor EL® from Sigma-Aldrich (Hamburg, Germany); Kolliphor HS15® was donated by BASF (Ludwigshafen, Germany); Labrasol Alf® and diethylene glycol monoethyl ether (Transcutol) was a gift from Gattefossè (Lyon, France); Hydroxypropyl-β-cyclodextrin (HP-β) from TCI (Qingdao, China); Sulfobutylether-β-cyclodextrin (SP-β) from Sigma-Aldrich (St. Louis, MO, USA); glycerol from Sigma-Aldrich (Petaling Jaya, Malaysia); propylene glycol from Sigma-Aldrich (St.

Table 1
List of investigated LNG samples obtained from different sources, batch number and the purity stated by the supplier.

Supplier	Reported purity	Batch No.
OOI Chemical (OOI)	99.8%	240,301
A2B Chem (A2B)	95%	2247,485
BOC Sciences (BOC)	99.88%	B23LM02161
LGC Mikromol (Mikromol)	98.7%	G1186122
MedChemExpress Europe (MCE)	99.88%	14,149
Target Mol	99,79%	115,871
Thermo Scientific (Thermo)	98%	461,100,010
Biosynth	> 99%	0000,030,008
Selleck	99.9%	S172705010001
MuseChem (Muse)	98%	M23 × 12,085
Wuhan Fortuna Chemical (Wuhan)	99.82%	20,221,221

Louis, MO, USA); polyethylene glycol 400 (PEG 400) from Thermo Scientific (Hamburg, Germany); sodium dodecyl sulfate (SDS) from VWR (Lutterworth, UK), cetyltrimethylammonium bromide (CTAB) from Thermo Scientific (Hamburg, Germany); phosphate buffered saline tablet from Sigma-Aldrich (St. Louis, MO, USA); 2F Powder for FaSSIF/FeSSIF from Biorelevant (London, UK). Water used throughout the studies was obtained from an Ultrapure Water dispenser 18.2 MΩ Millipore from Merck (Darmstadt, Germany).

2.2. Methods

2.2.1. NMR spectroscopy

All liquid-state NMR analyses were performed at 11.7T on a Jeol JNM-ECZ500R/S1 500 MHz NMR spectrometer (Kobe, Japan) equipped a Royal HFX probe. The samples were dissolved in deuterated DMSO and the ^{1}H NMR and ^{13}C NMR were performed with 128 and 4096 scans, respectively.

Solid-state NMR (ssNMR) analyses were performed at 16.4 T on a Bruker Avance IIIHD spectrometer (Billerica, MA, USA) equipped with a 4 mm HXY MAS probe at a 12 kHz MAS rate. Carbon spectra (^{1}H–^{13}C CP) were acquired with 3000 scans, a relaxation delay of 2.5 s and an acquisition time of 50 ms. The cross polarization (CP) was optimized on U–^{13}C,^{15}N L-alanine with a 30% ramp on the ^{13}C rf channel and Spinal64 was used for ^{1}H decoupling during acquisition with and rf field strength of 100 kHz. Chemical shifts were calibrated indirectly through the adamantane peak observed to low frequency (29.5 ppm relative to tetramethylsilane).

2.2.2. Attenuated total reflection Fourier transform infrared spectroscopy (ATR-FTIR)

FTIR spectra were collected in the range of 4000 – 650 cm^{-1} on an Agilent Cary 360 FTIR Spectrometer (Wilmington, DE, USA) with a Diamond-ATR module in reflectance mode. The spectra were collected from 32 co-added scans, with a spectral resolution of 2 cm^{-1}.

2.2.3. Raman spectroscopy

The solid-state Raman spectra were collected on a system consisting of an Ocean Optics immersion probe coupled to a B&W tek 785 nm fiber coupled laser and an Ocean Optics QEPro Raman spectrometer with a spectral resolution of 12 - 14 cm^{-1} (Peabody, MA, USA). 200 mW of laser power was used on the sample with an integration time of 1 s.

2.2.4. Powder X-ray diffraction (XRPD)

X-ray diffractograms were collected using a Rigaku Miniflex 600 X-ray diffractometer (Tokyo, Japan) with a voltage of 40 kV and a current of 15 mA from 5 to 60° (2θ angles) in reflection mode, with a step size of 0.02° and 5°/min. All samples were packed on the top of glass sample holders with the same depth for intensity comparison. The interlayer D-spacing of reflections were calculated using Braggś law ($n\lambda = 2d\sin\theta$) in which n is the order of diffraction, λ the wavelength (Cu Kα radiation; λ = 1.5406 Å), θ is the diffraction angle and d the D- spacing.

2.2.5. Wide-angle X-ray scattering (WAXS) and small-angle X-ray scattering (SAXS)

WAXS and SAXS measurements were carried out using a XEUSS 3.0 SAXS/WAXS System (Xenocs, Sassenage, France) with a CuKα X-ray source (λ = 0.154 nm, Xeuss 3.0 UHR Dual source Mo/Cu, Xenocs, Sassenage, France) and Eiger2 4 M detector (Dectris Ltd., Baden Deattwil, Switzerland) with slit collimation. The apparatus was operated at 50 kV and 0.6 mA with sample to detector distance of 300 mm to access a q-range of 0.03–1.5 Å. Data acquisition time was 20 min. The solid-state detector acquires a 2D image, in which all scattering vectors (angles) in the described range correspond to respective pixels of the detector image. The exposure time was thus the same for all angles studied, as the scattering data was obtained simultaneously for all angles.

Samples were enclosed into 2.5 mm in diameter metal O-rings covered with two Kapton windows with 12.5 μm thickness. The scattered intensity was normalized to the incident intensity and was corrected for the background scattering from the empty sample holder. Calibration to absolute scale was used. The measurements were performed at ambient temperature of 20 °C.

2.2.6. Thermal analysis

2.2.6.1. Differential scanning calorimetry (DSC). The melting point of the 11 batches of LNG were analyzed using a DSC 250 from TA instruments (New Castle, DE, USA). Samples (2–3 mg) were hermetically sealed in standard aluminum pans, and the samples were subjected to a heating/cooling cycle from 25 °C up to 260 °C with a heating rate of 10 °C/min under a 40 mL/min nitrogen gas flow.

2.2.6.2. Thermogravimetric analysis (TGA). The thermogravimetric profile of the samples was obtained using a Thermogravimetric analyzer TGA 4000 from Perkin Elmer (Waltham, MA, USA). The sample (~12 mg) was added in an alumina (Al_2O_3) crucible and heated from 25 to 600 °C on a 20 °C min^{-1} rate. N_2 was used as purge gas.

2.2.7. Dynamic vapor sorption (DVS)

Dynamic vapor sorption (DVS) experiments were performed in a Discovery SA from TA Instruments (New Castle, DE, USA). To investigate the hygroscopicity of the samples, 50–60 mg LNG were pre-dried before exposed to isoactivity (isohume) measurements at 75%RH (25 °C) and the weight gain was recorded. Each experiment was performed in duplicates.

2.2.8. Scanning electron microscopy (SEM)

The samples were mounted on double-sided adhesive carbon tape fitted on aluminum stubs. They were then gold coated using a Polaron SC7640 Sputter Coater manufactured by Quorum Technologies (Laughton, UK). Images (tiff format, 10 s, 1024 × 768) were taken using a Zeiss Gemini 300 Field Emission Scanning Electron Microscope (Oberkochen, Germany) at set magnifications (x200, x2k and x7.5k) using the secondary electron detector at 20 kv acceleration voltage and 8.5 mm working distance.

2.2.9. Quantification method for solubility studies

Analysis of LNG was done with an adapted HPLC method previously reported (Zhao et al., 2020). In short, the mobile phase consisted of 50:50% (v/v) of acetonitrile and pure MilliQ® water. Chromatographic separation was carried out using a C18 column (Xbridge 150 × 3.5 mm ID, 4.5 μm) fitted with a C18 guard column at 30 °C. The flow rate was set at 1 mL/min, 20 μL volume injected and UV detection wavelength set to 240 nm. LOD and LOQ was determined to be 48.06 ng/mL and 145.64 ng/mL, respectively. The method was confirmed to be linear up to 5344 ng/mL.

2.2.9.1. Equilibrium solubility of LNG. The determination of the equilibrium solubility of LNG was performed at ambient temperature in several organic solvents, pharmaceutical vehicles, and dissolution media using the shake-flask method. Saturated solutions containing LNG were prepared by weighing LNG into a 4 mL glass vial followed by addition of 0.5 mL solvent. This was treated for 10 min using a Covaris S220 Focused-ultrasonicator (Massachusetts, USA) with cycles per bust (CPB) set to 1000, duty factor (DF) at 50% and power intensity (PIP) at 200 W and then placed under rotation for a minimum of 12 h at ambient temperature. If all added LNG was solubilised extra compound was added and the procedure repeated. After equilibration the samples were centrifuged twice; once at 1900 g using an Eppendorf Centrifuge 5810R (Hørsholm, Denmark) for 10 min (22 °C). The supernatant was collected and centrifuged again using an Ole Dich microcentrifuge 157.MP (Hvidovre, Denmark) at 20,000 g for 10 min at 22 °C. Afterwards, the

samples were diluted in the mobile phase. Each experiment was performed in triplicates.

The solubility of LNG was determined in the following organic solvents; ethanol, acetone, methanol, isopropanol, acetonitrile, ethyl acetate, 1,4-dioxane, diglyme, N-methyl-2-pyrrolidone (NMP), dimethyl sulfoxide (DMSO), tetrahydrofuran (THF), dichloromethane (DCM), dimethylformamide (DMF) and N, N-dimethylacetamide (DMA). The tested pharmaceutical vehicles and dissolution media investigated are provided in Table 2.

2.2.9.2. Purity investigation. A stock solution of a European Pharmacopeia LNG standard was prepared by dissolving 5 mg of LNG in 10 mL of acetonitrile. A standard calibration curve was then prepared from this stock solution by serial dilution in 50:50 (v/v) water/acetonitrile solution over a concentration range of 268.8ng/mL to 4000 ng/mL. Eleven stock solutions from the different batches were prepared by accurately weighing and recording the amount of LNG dissolved in acetonitrile. Each sample was then diluted to 800 ng/mL in 50:50 (v/v) water/acetonitrile. The peak area measured for each sample was divided by the area corresponding to 800 ng/mL of the European Pharmacopeia standard to calculate the % purity.

2.2.10. Stability of delivered polymorphic form in slurry experiments

The stability of LNG in several solvents was investigated by preparing slurries in DMF, THF, NMP and DMSO at 22, 30, 37 and 60 °C. Additionally, slurries were prepared in ethyl acetate, diglyme, diglyme: water 95:5 (v/v) and DCM at room temperature. After 2 days, the slurries were filtered, and the recovered solids were collected and analysed by XRPD.

2.2.11. Amorphization investigation

To investigate if the samples could be partially amorphous, a film-casting method was performed as an attempt to obtain amorphous LNG. Briefly, 26 mg of LNG was dissolved in 3 mL of DCM. The solution was pipetted onto glass slides at different temperatures (22 °C to 175 °C) and a film was formed. Subsequently, the samples were stored in a desiccator at ambient temperature, connected to a vacuum pump, and analysed by XRPD. The diffraction patterns were compared with the pure reference batch used for solubility determination.

2.2.12. Laser diffraction analysis

The particle size distribution of pure LNG was determined by laser diffraction using a Mastersizer 3000+ Ultra (Malvern Panalytical Ltd, Malvern, UK) equipped with a Hydro medium-volume wet dispersion unit. Measurements were conducted at ambient temperature with a stirring rate of 1750 rpm. Ultrapure water obtained from a Milli-Q® SQ-240 system (Merck, Darmstadt, Germany) was used as the dispersant. Suspensions were prepared by dispersing 50 mg of LNG in 1 mL 3% (w/v) poloxamer 188 solution, followed by rotation for 15 min to ensure wetting of the LNG particles. Measurement parameters were set to a refractive index of 1.571 and an absorption index of 0.01 for LNG, while a refractive index of 1.33 was applied for the dispersant. The lower limit of obscuration was set to 2% and the higher limit was set to 12%. To minimize agglomeration in the wet dispersion unit, samples were subjected to ultrasonication for 45 s, followed by 30 min of stirring in the wet dispersion unit prior to measurement. Each suspension was measured five times. Calculations of the particle size distribution were performed by the Mastersizer Xplorer (v5.30) software using the Mie theory and calculated as volume-based diameters e.g. Dv10, Dv50, and Dv90.

Table 2
List of pharmaceutical vehicles and dissolution media in which the thermodynamic solubility of levonorgestrel was investigated.

Media	Concentration (% w/v)
HCl (pH = 1.2)	
50 mM Acetate buffer (pH =4.5)	
50 mM PBS (pH = 7)	
FaSSIF/ FeSSIF	
Transcutol®	
NaCl	0.9%
Sucrose	10%
PEG 400	30 and 100%
Propylene glycol	30 and 100%
Glycerol	30 and 100%
Hydroxypropyl-β-cyclodextrin (HP-β)	5, 10 and 20%
Sulfobutylether-β-cyclodextrin (SP-β)	5, 10 and 20%
Kolliphor HS15	5, 10 and 20%
Sodium dodecyl sulfate (SDS)	0.5, 1, 2, 3 and 5%
Cetyltrimethylammonium bromide (CTAB)	0.5, 1, 2, 3 and 5%
Polysorbate 20	0.5, 1, 2, 3, 5 and 10%
Polysorbate 80	0.5, 1, 2, 3, 5 and 10%
Polyoxyethylene 23 lauryl ether (Brij 35®)	0.5, 1, 2, 3, 5 and 10%
Caprylcaproyl polyoxyl-8glycerides (Labrasol Alf®)	0.5, 1, 2, 3, 5 and 10%
Kolliphor EL® (Cremophor EL®)	0.5, 1, 2, 3, 5, 10 and 20%

3. Results and discussion

3.1. Solid-state analysis of LNG

According to current knowledge, LNG is polymorphic and can exist in different crystalline forms, based upon a polymorphic investigation of LNG reported by Cao and co-workers (2017). Form γ is reported to be the thermodynamically stable polymorphic form of LNG at ambient temperature, while the α and β forms are the metastable forms (Cao et al., 2017). This conclusion was based on exposure of the three forms to elevated temperature (60 °C), high humidity (92.5%), light exposure (4500 lx) for 10 days, combined with placement of the three crystal forms under pressures of 19.6, 39.2, and 78.4 kN. Under these stress conditions, Cao and coworkers (2017) reported that the γ-form was the stable crystal form, whereas the α and β-forms were metastable and transformed into the γ-form under these conditions.

Cao and coworkers (2017) reported that the IR spectra of the α and β forms overlap and hence cannot be distinguished by IR spectroscopy, whereas the γ form should show an additional peak at 1046 cm^{-1} near the 1065 cm^{-1} and a broader band at 3300 cm^{-1} (Cao et al., 2017). The crystal form of the LNG samples from different suppliers obtained for the present study were therefore investigated by ATR-FTIR and Raman spectroscopy and the obtained spectra are presented in Fig. 2 and Fig. 3, respectively.

The IR spectra of the different LNG batches were superimposable (see Fig. 2), with no shifting in the absorption bands and presented similarities with the α and β forms previously reported by Cao et al. (2017). The O—H stretching vibrational modes, ν(O—H), were detected as a broad band at 3332 cm^{-1} and only one band at 1064 cm^{-1} was observed. The latter was assigned to the stretching vibrations of the bond formed between carbon and the oxygen from the hydroxyl group, ν(C—O). Furthermore, the stretching vibrations of the C—H bonds, ν(C—H) are

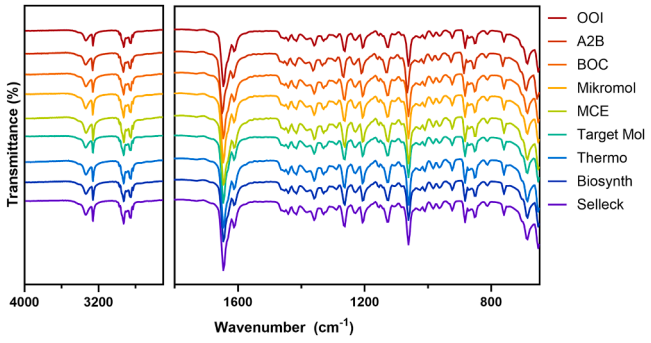

Fig. 2. Overlay of the ATR-FTIR curves for the different LNG batches. No significant difference was observed in the absorption bands.

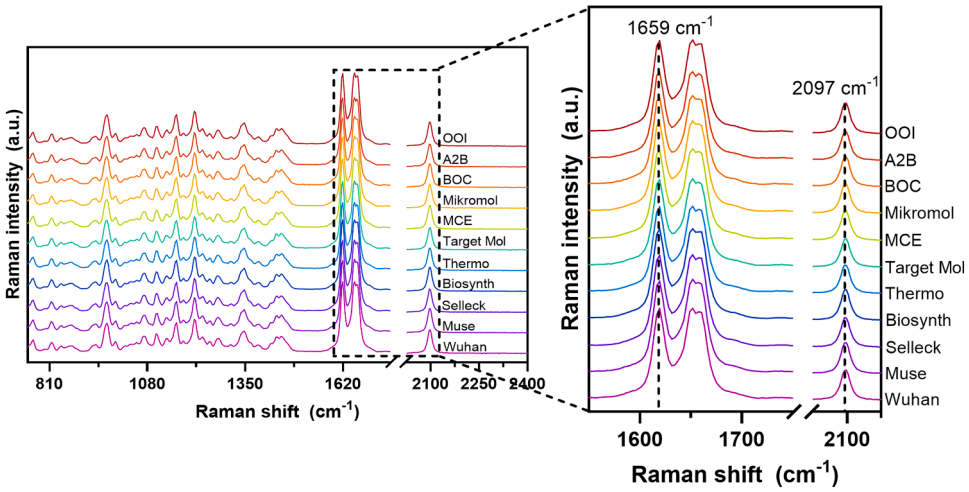

Fig. 3. Overlay of the Raman spectra of the LNG powder obtained from the different suppliers. No significant shift was observed in the vibrational modes of the different LNG batches.

detected as a band at 3258 cm^{-1}, while the bands in the spectral region of 2926 - 2850 cm^{-1} are due to the asymmetric C—H stretching vibrations in the cycloalkanes, ν(C—H). Finally, the C = O stretching vibrations, ν(C = O), were determined by an intense band at 1645 cm^{-1}. Ridichie and coworkers also reported characteristic LNG bands at 3342 cm^{-1}, 3267 cm^{-1}, 1651 cm^{-1} and 1067 cm^{-1} that were assigned to ν(O—H), ν(C—H), ν(C = O) and ν(C—O) modes, respectively (Ridichie et al., 2024, 2023).

Although IR spectroscopy has been proposed as a suitable technique for distinguishing the stable form from the metastable forms, the Raman spectra of α, β and γ forms have been reported to overlap completely (Cao et al., 2017). Hence, as expected, the Raman spectra of the different LNG batches (see Fig. 3) were identical, as it can be seen by the characteristic bands at 2097 cm^{-1} (symmetric -C≡C stretching modes, ν(C≡C)) and 1659 cm^{-1} (-C = C stretching modes, ν(C = C)). Furthermore, the bands in the spectral region of 1455–1388 cm^{-1} also overlapped and were attributed to the -CH_3 bending modes, δ(C—H) of LNG. The results indicated that the same crystal form was present in all investigated batches in the present study as no significant band shifting or peak broadening were observed, in accordance with previous reports (Fanse et al., 2021). Additionally, the sharp and well-defined peaks of LNG vibrational modes provided a strong indication of a high degree of crystallinity.

In addition to the IR and Raman spectra obtained for the batches obtained from different suppliers, the compounds were also investigated by XRPD (see Fig. 4), a technique that has also been reported to be capable of distinguishing the three reported polymorphic LNG forms (Cao et al., 2017). The X-ray powder diffraction patterns obtained in the present study showed intense reflections, indicating a high crystallinity character with no significant differences observed in the Bragg peaks for the different LNG samples.

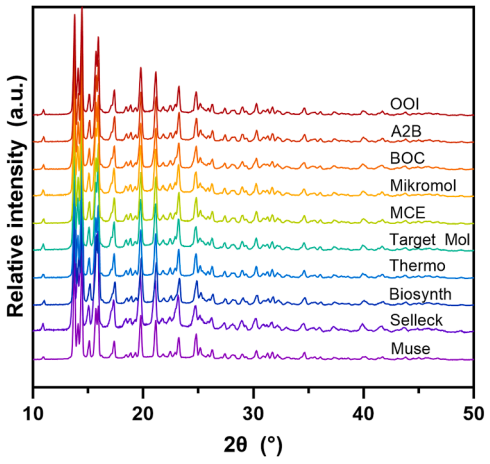

Fig. 4. Diffraction patterns of the LNG powder obtained from the different suppliers. No significant difference was observed.

Additional SAXS/WAXS measurements (see Fig. 5) were performed, confirming the matching phase purity across the different batches, as suggested by the XRPD results. Comparing the position of the most intense XRPD peaks from the OOI batch with the Bragg peaks assigned to the γ form by Cao and coworkers (see Supporting Information, Table S1) suggested that the polymorphic form present across the different LNG batches was the form denoted as the γ form by Cao et al. (2017). However, these results were in contrast with the data obtained by ATR-FTIR, in which the different LNG batches did not exhibit an additional peak at 1046 cm^{-1} near the 1065 cm^{-1} and a broader band at 3300 cm^{-1} characteristic of the γ form (Cao et al., 2017).

Cao and coworkers (2017) characterized the three existing crystal forms of LNG using DSC and reported a single sharp endothermic peak (melting point, T_m) which was detected in all three crystal forms, confirming the absence of solvent or water of crystallization. An endothermic peak at 239.2 °C was reported for the stable form, γ, while the two metastable forms, α and β, were reported to have endothermic peaks at 238.1 °C and 239.4 °C, respectively. However, the DSC method could not be used as a discriminative method since the difference between the melting points of forms β and γ was <1 °C (Cao et al., 2017). The melting temperatures and heat of fusion of the different LNG batches were determined by DSC in the present study (see Table 3) and the DSC thermograms are reported in the Supporting Information (see Fig. S1 – S10). Only one endothermic peak was identified in each LNG sample, with values in the range of 237.8 to 241.4 °C in accordance with the temperature range previously reported in the literature for LNG (Bao et al., 2018; Cao et al., 2017; Ridichie et al., 2023). Initially, the samples from Mikromol, Target Mol and A2B had the lowest melting points compared to the other batches. For that reason, a second run was performed and only Target Mol and Mikromol remained with the lowest T_m. The presence of impurities and the influence of particle size could potentially explain differences in melting points between samples, which will be discussed below for the two batches.

A close investigation of the DSC thermograms suggested that the melting of LNG could be concurrent with its decomposition. The enthalpy of fusion obtained from the integration of the melting peak therefore seemed to correspond to both the energy required to melt the

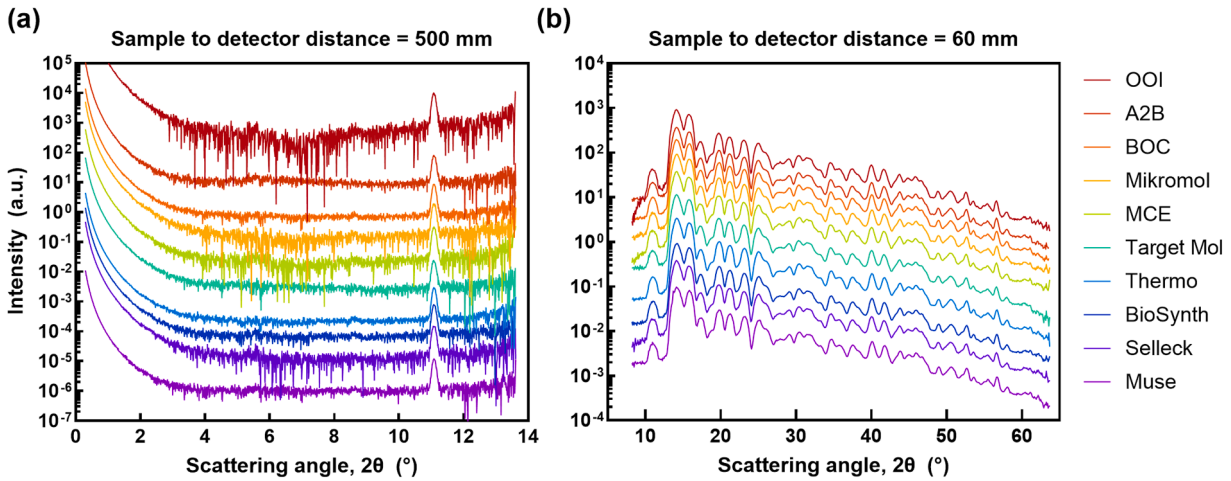

Fig. 5. SAXS (a) and WAXS (b) measurements of 10 different batches of LNG.

Table 3
DSC parameters from the different LNG batches.

Batch	First run		Second run	
	Peak onset	Enthalpy	Peak onset	Enthalpy
	[°C]	[J/g]	[°C]	[J/g]
OOI	240.0	131.5	240.4	115.4
Target Mol	237.8	116.4	238.6	123.8
Mikromol	238.9	143.0	239.3	101.5
A2B	239.9	113.5	240.5	144.9
BOC	241.4	138.7		
Thermo	241.1	132.5		
Muse	240.6	121.4		
MCE	240.3	125.5		
Selleck	240.3	125.1		
Biosynth	240.1	125.9		

compound as well as the energy associated with its decomposition.

Overall, the thermogravimetric (TGA) profiles of the different LNG batches displayed two major decomposition events, except for the batch from Muse (see Fig. 6). The sample from Muse was the only batch that displayed three major decompositions in the TGA run (see Fig. 7). Particle size, presence of impurities and crystal habit are generally the main factors affecting the kinetics of phase transitions (Giron, 1995). In this work, the thermogravimetric curves of LNG presented differences that most likely can be explained by the differences in the content of impurities, residual solvent, and particle size distribution of the sample, which will be discussed further below. Since the mass losses were detected above 235 °C, the differences in the thermogravimetric profiles cannot be attributed to the presence of water or residual solvent from the crystallization. Moreover, no mass loss below 100 °C was observed in the thermogravimetric profile of the LNG samples, confirming the DSC results, which suggested that the samples did not contain water adsorbed within the surface of the drug particles.

The TGA results from the present study also showed thermal stability up to 190 °C for most of the LNG samples, including the batch from Muse. The considerable thermal stability observed for all the LNG samples can be attributed to its conjugated and saturated scaffold and the grafted moieties (i.e. ketone and hydroxyl) that can form intermolecular H-bonds, stabilizing the crystal lattice (Ridichie et al., 2023).

The detail description of the decomposition events of the samples from OOI and Muse are reported in Table 4. In the first degradation step, LNG lost 26.5 and 34.5 wt % for the OOI and Muse batch, respectively, displaying considerable increase in mass loss as temperature increased. The TGA data obtained from the Muse batch was in accordance with the findings reported by Ridichie and coworkers (2024), in which LNG displayed thermal stability up to 185 °C and decomposition process characterized by three events (Ridichie et al., 2024). However, Ridichie et al. also reported that, in the first decomposition, LNG lost more than half of its mass (Ridichie et al., 2024). With the exception of the Muse sample, the present findings were in accordance with the previous work

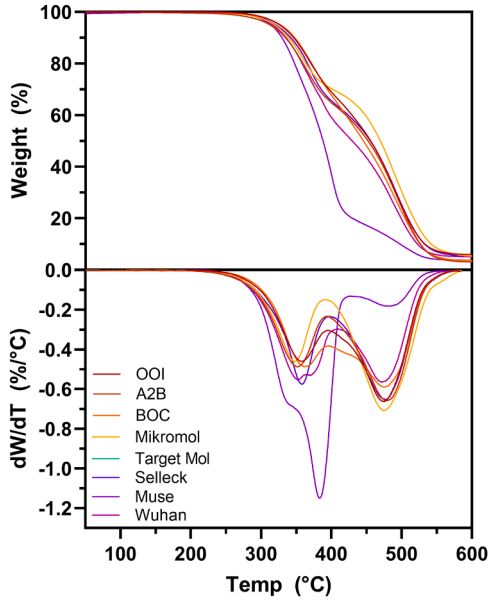

Fig. 6. Thermogravimetric profile of the different LNG batches. All samples display two decomposition events, while the Muse batch is the only one that shows three events.

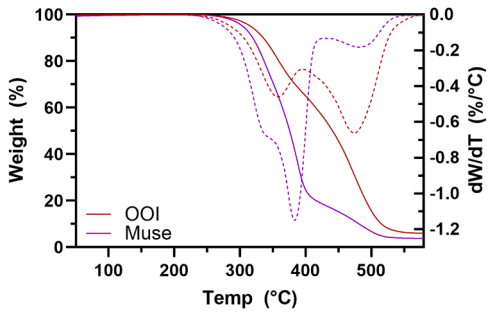

Fig. 7. Thermogravimetric profile of the OOI sample (red) and the Muse sample (violet).

Table 4
Detail description of the temperature intervals in which a weight loss was observed for the Muse and OOI samples.

Muse		OOI	
Temperature Interval (°C)	Weight loss (%)	Temperature Interval (°C)	Weight loss (%)
245.5 - 346.5	26.5	250 - 397.5	34.5
346.5 - 427.5	55.5	397.5 - 580	59.8
427.5 - 580	14.3	-	-
Residue	3.7	**Residue**	5.7

conducted by Ridichie et al. (2023), in which the thermal profile of LNG exhibited a two-step degradation process, characterized by a considerable increase in mass loss with the temperature evolution (Ridichie et al., 2023).

The results from the purity assessment determined using HPLC suggested high purity for Target Mol and Mikromol samples (see Table 5), indicating that the small variation in melting point observed in the DSC results might be associated with differences in particle size, instead of the presence of impurities. The Muse sample displayed a lower experimental purity compared with the OOI batch which, in principle, could explain the differences between the thermogravimetric profiles of the Muse and the OOI. However, the batches from A2B, MCE, and BOC also displayed lower purity values and still displayed two decomposition events. Therefore, the different decomposition profile of the sample from Muse was most likely due to the influence of the particle size or presence of residual solvents.

To confirm the high purity results obtained experimentally by HPLC and to better understand the differences in the thermal properties observed for some of the LNG batches, A2B, Mikromol, OOI, Target Mol and Wuhan batches were selected for further liquid-state NMR analysis. The ^{13}C NMR spectra of the different samples seemed to be identical. As expected, 20 distinct signals were detected in each spectrum, with the last signal (i.e. 40 ppm) most likely being overlapped by the DMSO signal (see Supporting Information. Fig. S11). In the ^{1}H NMR spectra, integrals added up to the expected 28 H atoms (see Supporting Information. Fig. S12 – S17). The signal at 5.7 ppm was attributed to the alkene proton, 5.3 ppm corresponded to the OH proton that was visible, since the solvent used was DMSO, and the signal at 3.33 ppm was attributed to the acetylenic proton. The intense signal at 3.35 ppm was correlated to the water in DMSO and the residual DMSO-d5 signal was observed at 2.50 ppm. Finally, the signals below 2.5 ppm corresponded to all the aliphatic protons, with the methyl group of the side chain clearly visible as a triplet at 0.92 ppm. The assignments were in accordance with previously reported ^{1}H NMR data of LNG with $CDCl_3$ as the solvent (ChemicalBook, 2017). Some changes in chemical shift were observed, most notably for the acetylenic proton but those might be explained by the OH proton exchanges with $CDCl_3$ which disappears in the spectrum. Overall, no detectable differences were observed between the liquid state NMR data of A2B, Mikromol, OOI, Target Mol and Wuhan batches. Moreover, all the samples displayed high purity with no detectable signals other than the ones from LNG.

Table 5
Purity values obtained experimentally using HPLC.

Batch	Expected purity[a]	Experimental purity[b]
A2B	95%	96.2%
Biosynth	> 99%	99.1%
BOC	99.88%	95.5%
MCE	99.88%	96.9%
Mikromol	98.7%	100.2%
Muse	98%	96.9%
OOI	99.8%	102.3%
Selleck	99.9%	97.8%
Target Mol	99.79%	102.5%
Thermo	98%	97.3%
Wuhan	99.82%	100.6%

[a] Information provided by the suppliers without details on the analytical procedures applied.
[b] Calculated relative to a PhEur standard.

The ssNMR spectra of the LNG batches from OOI, A2B and Target Mol are reported in the Supporting Information (Figures S18 and S19). The ssNMR spectrum of the sample from Target Mol displayed a broadening of the methyl peak line (see Fig. S20) and a shoulder on the aldehyde/ketone peak (see Fig. S21), while all the other peaks from the tested samples completely overlapped. Often, NMR line widths can be correlated with magnetic susceptibility (Nelson et al., 2006). However, the other peaks of the sample from Target Mol did not show a similar trend to the methyl peak, suggesting that it was unlikely a case of susceptibility broadening. The same logic can be applied to the size of the single crystal domains from the different batches. It is known that the presence of crystal defects contributes to changes in the apparent domain size of the crystal, which might also be correlated with the NMR line width (Nelson et al., 2006). Nevertheless, one should expect that a sample with reduced crystal quality would display changes in the line width of all peaks, and not just the methyl peak. Therefore, the differences in the ssNMR spectrum of the Target Mol sample, compared to the other samples from OOI and A2B, could be potentially associated with the presence of another crystalline.

Intrinsic physical properties of a drug compound such as hygroscopicity can be directly related to the drug stability and processability (Byrn et al., 2010). Therefore, knowing how much moisture the drug compound acquires at a given RH is needed to design specific formulation and packaging to ensure the stability of the finished product when shipped or stored at different environmental conditions (Bharate and Vishwakarma, 2013). The DVS curves can provide relevant information about the hygroscopic nature of solid species. It is often used to investigate hydrate formation and the water-absorption behaviour of the crystal forms. The DVS curves of the different LNG batches subjected to a constant 75% RH showed a small mass change (%) as a function of the time provided in the Supporting Information (see Fig. S20 – S25). The results suggested that the LNG batches are nonhygroscopic with <0.012% w/w weight gain observed across all investigated batches. According to the European Pharmacopeia, a compound is considered slightly hygroscopic if it shows <2% mass gain when stored at 25 °C for 24 h at 80% RH (Niazi, 2019), as was observed for LNG samples in the present study. Therefore, the compound can be described as non-hygroscopic. For that reason, the investigation of the dehydration and the hydration behaviour by the conventional vapor sorption-desorption isothermal cycles were not further conducted.

Particle size distribution of LNG drug particles is another factor that may be affected by API source variation. For instance, LNG particles in microneedle patches remain in the solid state, and therefore the particle size may have impact on product performance, particularly the dissolution rates (Bao et al., 2020). To investigate the particle size distribution of some of the supplied batches, a wet dispersion analyses were performed on LNG batches from A2B, Biosynth, Mikromol, OOI, and Wuhan when dispersed in 3% (w/v) poloxamer 188. The particle size distribution data for the LNG batches were not provided by the suppliers, with exception of the batch from Wuhan. The results reported in Fig. 8. and Table 6 display the particle size distributions for the different batches.

Initial measurements exhibited a bimodal distribution, with the primary volume fraction observed in the smaller size range of approximately 5–8 μm, and a secondary, but smaller volume fraction at around 70–100 μm. The presence of large particles was not observed in the SEM images, see supporting information (Figure S26 and S27). Despite a large difference in the number of particles analysed by the two methods, this could suggest that the larger particles detected by laser diffraction were possibly a result of agglomeration occurring during the addition of the sample to the wet dispersion unit as the sample was diluted in the wet dispersion unit. Therefore, the particles may not be sufficiently wetted by the stabilizer resulting in attraction forces between the

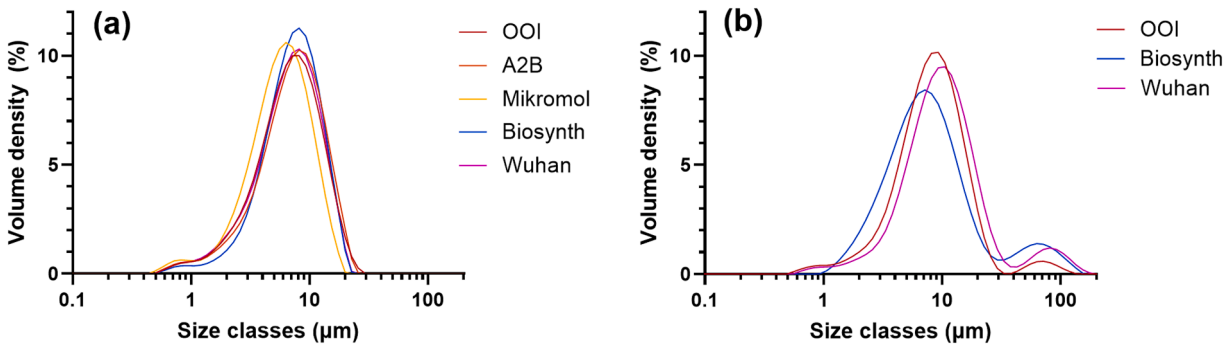

Fig. 8. Particle size distributions of LNG from Mikromol, Wuhan, A2B, OOI, and Biosynth dispersed in 3% (w/v) poloxamer 188. (A) Samples subjected to stirring and ultrasonication. (B) Samples measured immediately after addition to the Mastersizer.

Table 6
Particle sizes from A2B, Biosynth, Mikromol, OOI, and Wuhan batches.

Batch	D (10) [μm]	D (50) [μm]	D (90) [μm]	D (99) [μm]	Span
A2B	2.77	7.32	14.3	20.5	1.579
Biosynth	3.22	7.28	13.5	18.5	1.414
Mikromol	2.41	5.78	11.2	16.1	1.515
OOI	2.64	6.86	13.8	20.9	1.630
Wuhan	2.59	6.93	13.5	18.7	1.569
Wuhan	0.9 [a]	2.0 [a]	7.0 [a]	16 [a]	

[a] Declared by the supplier.

particles. The software fit was also evaluated, as an incorrect refractive index or absorption index could have influenced the results. However, the fit was found to be satisfactory with weighted residuals and residuals of approximately 0.5%. The software evaluates the goodness-of-fit based on residuals and weighted residuals preferably below 1% depending on particle sizes and the distribution width. To minimize agglomeration, samples were subjected to stirring in the wet dispersion unit 30 min prior to measurement, which reduced the secondary peak associated with the larger particles, while the primary peak remained unchanged, suggesting that it did not affect the amount of LNG being solubilized. To further break up the agglomerates, ultrasonication of 45 s was applied prior to the 30 min of stirring. Ultrasonication resulted in additional reduction of the secondary peak but did not shift or reduce the primary peak. These findings confirm that the primary peak associated with the smaller particles remained intact, while the larger particles originated from reversible agglomerates from the sample preparation or as an artifact of the measurement method.

To better understand the differences obtained in the thermal analysis and to confirm the measured particle size distribution obtained by laser diffraction, the morphology of the selected batches, namely A2B, OOI, Mikromol, Muse, Target Mol and Wuhan, were investigated with scanning electron microscopy and the SEM micrographs are provided in the Supporting Information (see Fig. S1 and Fig. S2). Interestingly, unlike the present findings, another study reported neat, micronized LNG particles from a different supplier with a flake-like shape and a broad particle size distribution determined by image analysis (Farahmandghavi et al., 2019). Overall, there was no indication of significant differences in terms of morphology for most of the samples tested. Nonetheless, the samples from Target Mol and Mikromol displayed slightly smaller particle sizes, which could explain the differences in melting points compared to the other batches. Collectively, these results suggest that there is a small risk of receiving different polymorphic forms of LNG independent of the supplier, indicating a low solid-state risk associated with changes in the source of the API.

3.2. Investigation of polymorphic stability

Investigating the polymorphic behaviour of a drug is an important part of the preformulation stage. Solubility, dissolution rate, stability, hygroscopicity and solid-state reactivity are some of the physicochemical properties affected by polymorphism. However, the biggest impact is often associated to the bioavailability, especially is the case of dissolution-limited absorption mechanisms (Giron, 1995). For that reason, rapid polymorphic screening process is often performed to identify all possible crystal forms, including solvates, hydrates, and select the stable form that can be formulated into a desired dosage form (Byrn et al., 2010). A polymorphic screen of LNG was previously conducted by Cao and co-workers (2017), who reported three different polymorphic forms, as mentioned above. In the present work, an attempt was made to reproduce these three forms based on the experimental procedures described by Cao et al. (2017). However, in all cases, only the γ-form was observed, as confirmed by the XRPD diffractogram. The corresponding IR spectra matched that shown in Fig. 2 but lacked the additional peak at 1046 cm^{-1} reported by Cao et al. (2017) for the γ-form. It was not clear why the work by Cao and co-workers (2017) could not be reproduced, however, as the focus of the present work was to investigate the stability of the supplied γ-form, the LNG sample from OOI was selected for slurry experiments in a variety of solvents commonly used in polymer-based pharmaceutical formulations to assess potential polymorphic conversions. The XRPD analysis showed that no physical transformations occurred after stirring LNG in NMP, DMF THF and DMSO at different temperatures, see Fig. 9. Similar experiments were also conducted with the LNG liberated according to the procedures described by Cao et al. (2017) and similar data was observed (data not shown).

Identical diffractograms were also obtained for the products of the slurry experiments conducted in ethyl acetate, diglyme, diglyme: water (95:5) w/w and DCM, at room temperature (see Fig. 10). The absence of solvate formation has been attributed to a weaker solvent-solute affinity relative to the solute-solute and solvent-solvent affinities (Boothroyd et al., 2018). Accordingly, the XRPD results obtained from the slurry products prepared in the selected solvents suggested a weak affinity between LNG and the organic solvents, confirming the compound's pronounced physical stability, as previously indicated by the thermal analysis. The investigations with the elevated temperature suggest that pharmaceutical processing with a slurry of LNG in the investigated solvent most likely would not induce any solid form conversion.

Amorphous forms may be obtained by solvent-based methods, melting or grinding, with the solvent-based methods being the most widely used (Byrn et al., 2010). In this present worked, a solvent-based method was performed by dissolving LNG in DCM (b.p. = 39.6 °C) and melt-casted to form thin films on a pre-heated glass slide at different temperatures (22 – 175 °C). After being dried under vacuum, the samples were analysed with XRPD measurements. Despite the fast solvent evaporation rate, it was not possible to induce amorphization and no broad diffraction pattern (halo) was observed with the increase in the temperature. The X-ray diffraction patterns (see Fig. 11) indicated a

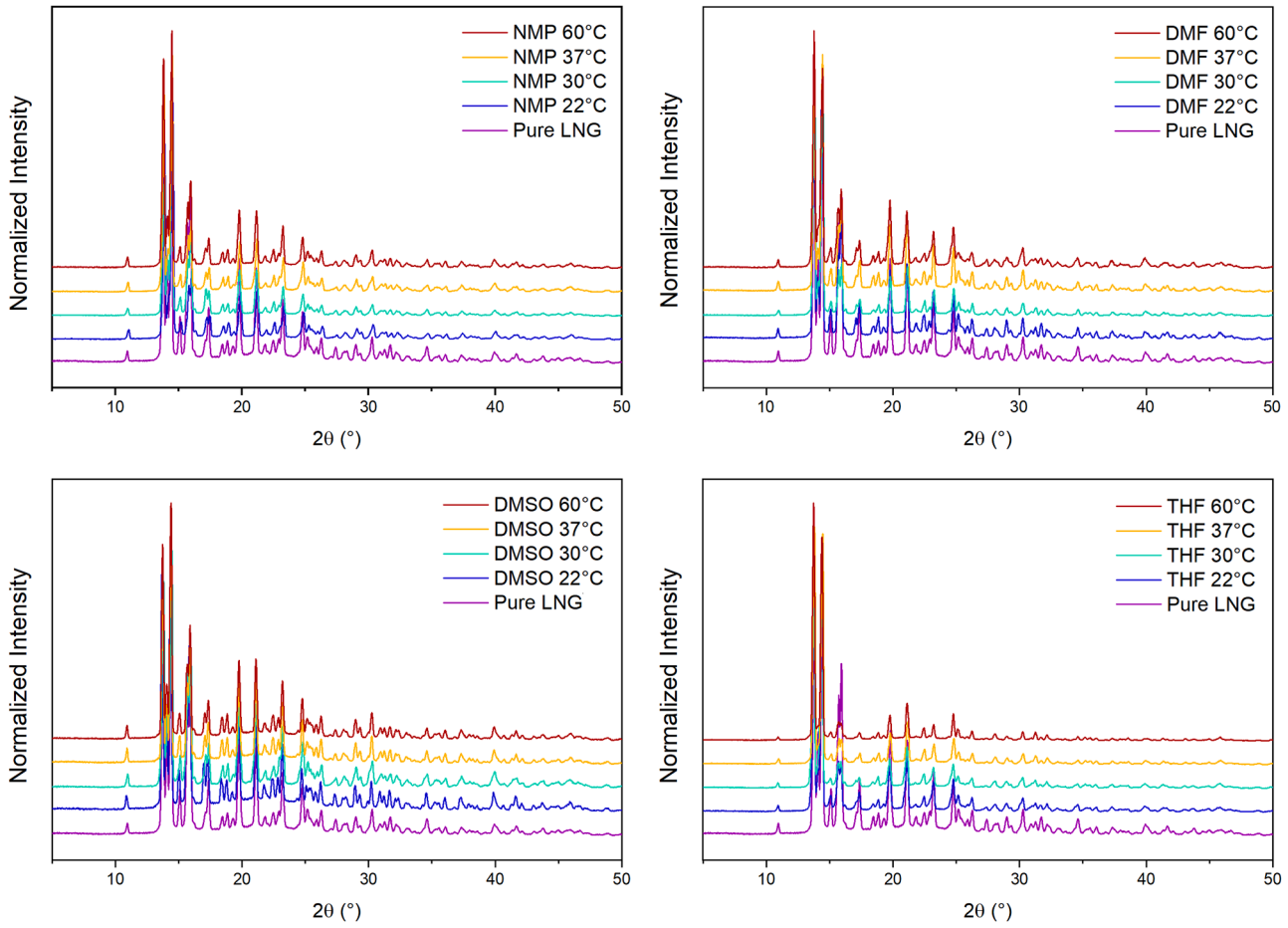

Fig. 9. XRPD of the LNG products obtained from the slurry experiments in a) NMP b) DMSO c) DMF and d) THF at 22 °C, 30 °C, 37 °C and 60 °C. The results show identical diffractograms, indicating that no polymorphic conversion occurred.

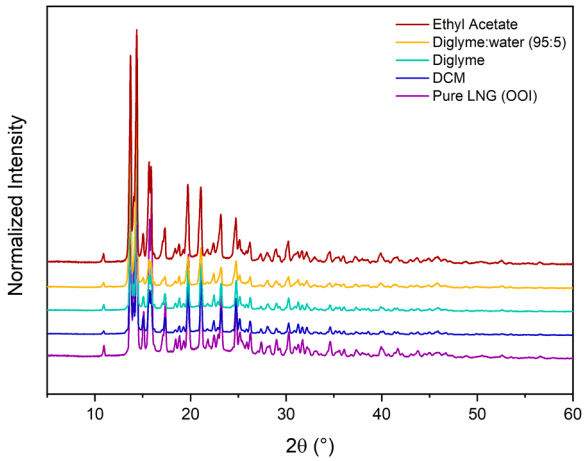

Fig. 10. XRPD of the products obtained from the slurry experiments of LNG conducted in different solvents at room temperature. The diffractograms overlap, indicating that no polymorphic conversion occurred.

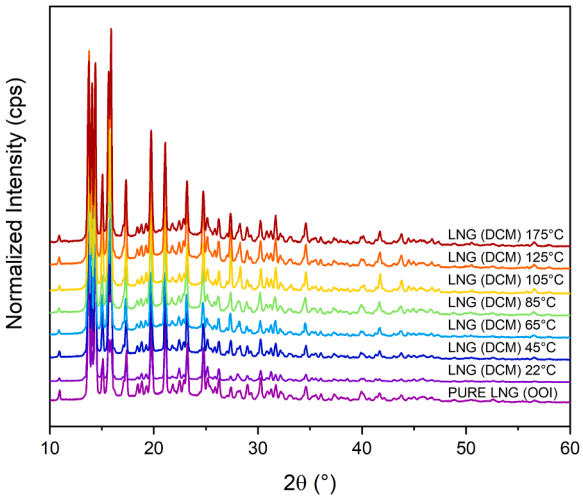

Fig. 11. XRPD of the dried LNG obtained from a melt-casting method performed in DCM at different temperatures. The lack of a halo in the diffractogram indicates the strong tendency of LNG to remain in the crystalline state.

strong tendency of LNG to remain in the crystalline form and the same diffraction patterns observed as the starting material, making it difficult to obtain a 100% amorphous LNG sample.

These investigations indicate that the crystalline stability of LNG in the γ-form was very high and that processing suspensions of the compound in different organic solvents, as well as exposure to elevated temperatures, does not induce polymorphic transformation. Pharmaceutical processing therefore appears to present a low risk with respect to solid-stage changes.

3.3. Solubility of LNG in organic solvents, pharmaceutical vehicles and dissolution media

Solubility testing of the stable polymorphic form is essential in reaching proper decision making in the formulation development stage (Byrn et al., 2010). Conventional solubilization techniques include cyclodextrin inclusion and the use of surfactants and cosolvents. The type and concentration of surfactants can determine the solubilizing ability, but also toxicity. For instance, cationic surfactants present higher toxicity while nonionic surfactants are the least toxic. Another widely used solubilization approach is the addition of cosolvents, which are often water-miscible organic solvents such as ethanol, propylene glycol, DMSO and PEG, with a solubilization mechanism based on decreasing the solvents mixture polarity to enhance its compatibility with a nonpolar solute (Xie et al., 2024). In summary, pharmaceutical vehicles and organic solvents are often used to solubilize LNG for formulation development purposes, as well as pharmacokinetic and drug release research. For instance, release media containing 20% v/v of ethanol, isopropanol or THF have been used in accelerated *in vitro* drug release studies from intrauterine systems (Bao et al., 2019). Other solvents such as DCM can be used as organic phase in microemulsion-evaporation techniques to increase drug loading in nanoparticles containing LNG, while ethyl acetate mixed with ethanol was found to significantly enhance LNG flux and skin permeability relative to saline solution (Catz and Friend, 1990; Farahmandghavi et al., 2019). Finally, solvents such as DMF, DMSO, THF and 1,4-dioxane have been widely used in microneedle manufacturing (Kang et al., 2022; Yavuz et al., 2020).

The LNG solubility data in a variety of organic solvents are reported in Table 7, while the LNG concentration in different pharmaceutical vehicles and dissolution media is reported in Table 8.

The equilibration method used in the present study included an initial treatment by focused ultrasound to reduce particle size (Zulbeari and Holm, 2024) and thereby enhance the dissolution process. Following this, samples were left to equilibrate for at least 12 h in the presence of excess crystalline LNG in the vial to allow time for the system to reach equilibrium. The data presented above, indicating the high stability of the solid form of LNG, supported that the likelihood of this protocol inducing amorphization and thereby supersaturation was low.

In the presence of organic solvents, the results indicated that LNG exhibited the highest solubility in NMP, followed by DMA, DMSO, and DMF, in comparison with the other organic solvents evaluated.

Interestingly, the solubility of LNG in other solvents, such as 1,4-Dioxane, THF, and their mixtures, -with or without water- showed similar results, suggesting that these solvents could potentially be used to dissolve biodegradable polymers (e.g., poly (lactic-co-glycolic acid), PLA) for microneedle fabrication.

Table 7
LNG solubility in different organic solvents.

Batch	Solubility [mg/mL][a]
Toluene	2.52 ± 0.68
Acetonitrile	2.53 ± 0.02
Isopropanol	2.76 ± 0.48
Ethanol 96%	5.21 ± 1.10
Acetone	5.45 ± 0.89
Ethyl acetate	5.82 ± 1.64
Methanol	6.91 ± 0.23
Dichloromethane (DCM)	13.48 ± 1.35
Diglyme	13.08 ± 0.44
Diglyme: water 95:5 (v/v)	14.89 ± 0.79
1,4-Dioxane	32.58 ± 4.92
1,4-Dioxane: water 95:5 (v/v)	33.61 ± 0.75
Tetrahydrofuran (THF)	40.60 ± 5.08
1,4-Dioxane: THF: water 70:25:5 (v/v)	40.38 ± 1.67
Dimethylacetamide (DMA)	95.83 ± 4.00
Dimethylsulfoxide (DMSO)	57.56 ± 6.29
Dimethylformamide (DMF)	57.33 ± 7.14
N-methyl-2-pyrrolidone (NMP)	134.80 ± 5.10

[a] Mean ± standard deviation.

Since LNG is a very poorly water-soluble compound, the results in aqueous media without the presence of solubility enhancers were below the limit of detection of the equipment (LOD = 48.06 ng/mL). Therefore, slurry experiments performed in 50 mM Acetate buffer (pH = 4,5), 50 mM PBS (pH = 7), HCl solution (pH = 1.2) and the results for the stressed stability studies did not produce any relevant data. In fact, to investigate the dissolution rate and solubility of the three polymorphic forms of LNG in aqueous media, Cao and coworkers performed the measurements in 1% PS80 (Cao et al., 2017).

When comparing the solubility of different pharmaceutical vehicles at 100% w/v, the highest LNG concentration was achieved in Transcutol® followed by PEG 400. Among the surfactants tested within the 0.5 – 5% w/v range, LNG displayed considerable higher solubility in ionic surfactants, especially CTAB, relative to nonionic surfactants. The solubility of LNG in aqueous systems containing non-ionic surfactants (i.e. Brij 35®, Kolliphor EL®, Labrasol Alf®, PS20 and PS80), was highest in 10% Brij 35®, with a direct correlation between surfactant concentration and LNG solubility.

Overall, the LNG solubility data suggested that cyclodextrins are the most efficient solubility enhancers, particularly sulfobutylether-β-cyclodextrin. Moreover, a previous pharmacokinetic study of LNG in rats and minipigs demonstrated that parenteral formulations prepared with 10% hydroxypropyl-β-cyclodextrin in normal saline ensured drug stability and suitability for various parenteral routes (intravenous bolus or infusion, subcutaneous, and intradermal) (Ko et al., 2022). Therefore, this current work expands the database of LNG solubility values under varying conditions that might improve predictive drug loading and release profiles of novel formulations containing LNG.

4. Conclusions

Levonorgestrel (LNG) is a poorly water-soluble compound with limited polymorphic diversity. Although several preformulation studies have been conducted on LNG, a lack of comprehensive data regarding its solubility and physical stability in various solvents, pharmaceutical vehicles, and dissolution media remains. To address this, a thorough solid-state investigation of LNG from multiple sources was carried out to evaluate the potential impact of source variability. Spectroscopic analysis (i.e. FT-IR and Raman) and X-ray diffraction measurements indicated that all LNG samples exhibit pronounced crystallinity and consistent phase purity across all batches. Notably, the absence of polymorphic transitions following slurry experiments in various solvents indicates high physical stability of the compound, which was further confirmed by thermal analysis. Further, the analysis of LNG obtained from multiple suppliers generally provided consistent solid-state properties across the suppliers, which significantly would derisk development work made with LNG in different laboratories using the compound from different sources.

The solubility data of LNG reported in this study covered a range of pharmaceutical vehicles, organic solvents, and dissolution media, each employed to enhance LNG solubilization for formulation development, and to support pharmacokinetic studies and drug release investigations.

CRediT authorship contribution statement

Clarice Sombra de Medeiros: Writing – original draft, Validation, Methodology, Investigation, Formal analysis, Data curation, Conceptualization. **Magnus Ipsen Pedersen:** Writing – review & editing, Investigation, Data curation. **Mathias Dam Mønster Sørensen:** Writing – review & editing, Visualization, Methodology, Investigation, Data curation. **Chloe Hopper:** Data curation, Formal analysis, Writing – review & editing. **Martin Aage Barsøe Hedegaard:** Writing – review & editing, Methodology. **Sheng Qi:** Writing – review & editing, Visualization, Methodology, Data curation. **Zahari Vinarov:** Writing – review

Table 8
LNG solubility in different dissolution media and pharmaceutical vehicles.

Pharmaceutical vehicle/ Dissolution medium	Solubility[a] [μg/mL]					
FaSSIF	2.57 ± 0.07					
FeSSIF	8.82 ± 0.34					
10%w/v sucrose in water	4.59 ± 1.12					
Transcutol ®	6467.33 ± 684.80					
20% Kolliphor EL ®	153.06 ± 5.78					
PEG 400	30% [b]	100% [b]				
	18.51 ± 6.88	3255.54 ± 523.55				
Glycerol	30% [b]	100% [b]				
	46.72 ± 9.02	2360.16 ± 133.46				
Propylene Glycol	30% [b]	100% [b]				
	46.33 ± 16.48	2193.22 ± 370.70				
Hydroxypropyl-β-cyclodextrin	5% [b]	10% [b]	20% [b]			
	134.44 ± 4.91	244.96 ± 3.33	465.07 ± 8.01			
Sulfobutylether-β-cyclodextrin	5% [b]	10% [b]	20% [b]			
	305.43 ± 12.49	618.89 ± 25.02	1052.67 ± 32.47			
Kolliphor HS15®	5% [b]	10% [b]	20% [b]			
	41.64 ± 1.52	76.32 ± 0.61	135.80 ± 3.14			
SDS	0.5% [b]	1% [b]	2% [b]	3% [b]		
	60.95 ± 1.51	163.66 ± 6.96	365.96 ± 5.21	455.58 ± 9.74		
CTAB	0.5% [b]	1% [b]	2% [b]	3% [b]	5% [b]	10% [b]
	9.96 ± 0.14	30.87 ± 3.47	86.85 ± 3.35	104.17 ± 1.47	407.02 ± 27.27	430.01 ± 14.67
PS20	0.5% [b]	1% [b]	2% [b]	3% [b]	5% [b]	10% [b]
	6.96 ± 0.11	12.08 ± 0.46	18.44 ± 1.15	23.37 ± 0.91	35.78 ± 0.52	67.50 ± 0.36
PS80	0.5% [b]	1% [b]	2% [b]	3% [b]	5% [b]	10% [b]
	7.39 ± 0.18	13.16 ± 0.46	20.17 ± 0.47	25.84 ± 0.40	41.46 ± 0.57	78.28 ± 0.25
Labrasol Alf®	0.5% [b]	1% [b]	2% [b]	3% [b]	5% [b]	10% [b]
	1.86 ± 0.07	3.37 ± 0.10	15.57 ± 0.39	23.11 ± 1.53	37.37 ± 1.63	77.46 ± 1.47
Kolliphor EL®	0.5% [b]	1% [b]	2% [b]	3% [b]	5% [b]	10% [b]
	8.35 ± 0.01	13.89 ± 0.61	20.28 ± 1.08	28.99 ± 0.81	49.10 ± 0.15	88.49 ± 1.06
Brij 35®	0.5% [b]	1% [b]	2% [b]	3% [b]	5% [b]	10% [b]
	8.63 ± 0.16	15.49 ± 0.39	24.39 ± 0.51	32.19 ± 1.12	50.50 ± 1.20	96.19 ± 0.78

[a] Mean ± standard deviation.
[b] % w/v in ultrapure water.

& editing, Visualization, Methodology, Data curation. **René Holm:** Writing – review & editing, Supervision, Resources, Project administration, Methodology, Conceptualization.

Declaration of competing interest

The author is an Editorial Board Member/Editor-in-Chief/Associate Editor/Guest Editor for this journal and was not involved in the editorial review or the decision to publish this article.

Acknowledgements

This publication is based on research funded in part by the Gates Foundation, grant INV-073632. The findings and conclusions contained within the manuscript are those of the authors and do not necessarily reflect the positions or policies of the Gates Foundation.

Zahari Vinarov acknowledges the SWAXS instrument access, provided by the Center of Competence "Sustainable utilization of bioresources and waste of medicinal and aromatic plants for innovative bioactive products" BIORESOURCES BG, Grant BG16RFPR002-1.014-0001.

The authors thank Prof. Eric J. Munson from Purdue University and Prof. Michael Pedersen from the Southern University of Denmark for their support with the interpretation of the solid-state and liquid-state NMR data.

Supplementary materials

Supplementary material associated with this article can be found, in the online version, at doi:10.1016/j.ejps.2026.107562.

Data availability

Data will be made available on request.

References

Ayuk, B.E., Yankam, B.M., Saah, F.I., Bain, L.E., 2022. Provision of injectable contraceptives by community health workers in sub-Saharan Africa: a systematic review of safety, acceptability and effectiveness. Hum. Resour. Health 20, 66. https://doi.org/10.1186/s12960-022-00763-8.

Bao, Q., Gu, B., Price, C.F., Zou, Y., Wang, Y., Kozak, D., Choi, S., Burgess, D.J., 2018. Manufacturing and characterization of long-acting levonorgestrel intrauterine systems. Int. J. Pharm. 550, 447–454. https://doi.org/10.1016/j.ijpharm.2018.09.004.

Bao, Q., Zou, Y., Wang, Y., Kozak, D., Choi, S., Burgess, D.J., 2019. Drug release testing of long-acting intrauterine systems. J. Control. Release 316, 349–358. https://doi.org/10.1016/j.jconrel.2019.11.015.

Bao, Q., Zou, Y., Wang, Y., Choi, S., Burgess, D.J., 2020. Impact of product design parameters on in vitro release from intrauterine systems. Int. J. Pharm. 578, 119135. https://doi.org/10.1016/j.ijpharm.2020.119135.

Bearak, J.M., Popinchalk, A., Beavin, C., Ganatra, B., Moller, A.-B., Tunçalp, Ö., Alkema, L., 2022. Country-specific estimates of unintended pregnancy and abortion incidence: a global comparative analysis of levels in 2015–2019. BMJ Glob. Health 7. https://doi.org/10.1136/bmjgh-2021-007151.

Bharate, S.S., Vishwakarma, R.A., 2013. Impact of preformulation on drug development. Expert. Opin. Drug Deliv. 10, 1239–1257. https://doi.org/10.1517/17425247.2013.783563.

Boadu, I., 2022. Coverage and determinants of modern contraceptive use in sub-Saharan Africa: further analysis of demographic and health surveys. Reprod. Health 19, 18. https://doi.org/10.1186/s12978-022-01332-x.

Boothroyd, S., Kerridge, A., Broo, A., Buttar, D., Anwar, J., 2018. Why do some molecules form hydrates or solvates? Cryst. Growth Des. 18, 1903–1908. https://doi.org/10.1021/acs.cgd.8b00160.

Byrn, S.R., Zografi, G., Chen, X., 2010. Accelerating proof of concept for small molecule drugs using solid-State chemistry. J. Pharm. Sci. 99, 3665–3675. https://doi.org/10.1002/jps.22215.

Cao, J., Yang, D., Zhang, L., Du, G., Lyu, Y., 2017. Research on preponderant pharmaceutical polymorphs of Levonorgestrel. Her. Med. 36, 1339–1343. https://doi.org/10.3870/j.issn.1004-0781.2017.12.001.

Catz, P., Friend, D.R., 1990. Effect of cosolvents on ethyl acetate enhanced percutaneous absorption of levonorgestrel. J. Control. Release 12, 171–180. https://doi.org/10.1016/0168-3659(90)90093-9.

ChemicalBook, 2017. Levonorgestrel (CAS 797-63-7) 1H NMR spectrum [WWW Document]. URL. https://www.chemicalbook.com/SpectrumEN_797-63-7_1HNMR.htm (accessed 9.19.25).

Duijkers, I.J.M., Klipping, C., Rautenberg, T., Schug, B.S., Kochhar, P.S., Osterwald, H., Oettel, M., 2022. Effect on ovarian activity and ovulation inhibition of different oral dosages of levonorgestrel. Contraception 110, 6–15. https://doi.org/10.1016/j.contraception.2022.01.018.

Fanse, S., Bao, Q., Zou, Y., Wang, Y., Burgess, D.J., 2021. Effect of crosslinking on the physicochemical properties of polydimethylsiloxane-based levonorgestrel intrauterine systems. Int. J. Pharm. 609, 121192. https://doi.org/10.1016/j.ijpharm.2021.121192.

Fanse, S., Bao, Q., Burgess, D.J., 2022. Long-acting intrauterine systems: recent advances, current challenges, and future opportunities. Adv. Drug Deliv. Rev. 191, 114581. https://doi.org/10.1016/j.addr.2022.114581.

Farahmandghavi, F., Imani, M., Hajiesmaeelian, F., 2019. Silicone matrices loaded with levonorgestrel particles: impact of the particle size on drug release. J. Drug Deliv. Sci. Technol. 49, 132–142. https://doi.org/10.1016/j.jddst.2018.10.029.

Frost, J.J., Lindberg, L.D., 2013. Reasons for using contraception: perspectives of US women seeking care at specialized family planning clinics. Contraception 87, 465–472. https://doi.org/10.1016/j.contraception.2012.08.012.

Gipson, J.D., Koenig, M.A., Hindin, M.J., 2008. The effects of unintended pregnancy on infant, child, and parental health: a review of the literature. Stud. Fam. Plann. 39, 18–38. https://doi.org/10.1111/j.1728-4465.2008.00148.x.

Giron, D., 1995. Thermal analysis and calorimetric methods in the characterisation of polymorphs and solvates. Thermochim. Acta Pharm. Therm. Anal. 248, 1–59. https://doi.org/10.1016/0040-6031(94)01953-E.

Jain, J., Dutton, C., Nicosia, A., Wajszczuk, C., Bode, F.R., Mishell, D.R., 2004. Pharmacokinetics, ovulation suppression and return to ovulation following a lower dose subcutaneous formulation of Depo-Provera®. Contraception 70, 11–18. https://doi.org/10.1016/j.contraception.2004.01.011.

Kang, S., Song, J.E., Jun, S.-H., Park, S.-G., Kang, N.-G., 2022. Sugar-triggered burst drug releasing poly-lactic acid (PLA) microneedles and its fabrication based on solvent-casting approach. Pharmaceutics 14, 1758. https://doi.org/10.3390/pharmaceutics14091758.

Ko, P.J., Milad, M.A., Radulovic, L.L., Gibson, D.M., 2022. Pharmacokinetics of levonorgestrel and etonogestrel in rat or minipig following intravenous, subcutaneous, or intradermal administration. Xenobiotica 52, 575–582. https://doi.org/10.1080/00498254.2022.2079023.

Kook, K., Gabelnick, H., Duncan, G., 2002. Pharmacokinetics of levonorgestrel 0.75 mg tablets. Contraception 66, 73–76. https://doi.org/10.1016/S0010-7824(02)00321-9.

Li, W., Chen, J.Y., Terry, R.N., Tang, J., Romanyuk, A., Schwendeman, S.P., Prausnitz, M. R., 2022. Core-shell microneedle patch for six-month controlled-release contraceptive delivery. J. Control. Release 347, 489–499. https://doi.org/10.1016/j.jconrel.2022.04.051.

Nelson, B.N., Schieber, L.J., Barich, D.H., Lubach, J.W., Offerdahl, T.J., Lewis, D.H., Heinrich, J.P., Munson, E.J., 2006. Multiple-sample probe for solid-state NMR studies of pharmaceuticals. Solid State Nucl. Magn. Reson. 29 (1–3), 204–213. https://doi.org/10.1016/j.ssnmr.2005.08.006.

Niazi, S.K., 2019. Handbook of Preformulation: Chemical, Biological, and Botanical Drugs, 2nd ed. CRC Press. ed.

Rehman, Q., Akash, M.S.H., Imran, I., Rehman, K., 2020. Stability of pharmaceutical products. In: Akash, M.S.H., Rehman, K. (Eds.), Drug Stability and Chemical Kinetics. Springer, Singapore, pp. 147–154. https://doi.org/10.1007/978-981-15-6426-0_10.

Ridichie, A., Ledeţi, A., Peter, F., Ledeţi, I., Muntean, C., Rădulescu, M., 2023. Kinetic investigation of the oxidative thermal decomposition of levonorgestrel. Processes 11, 3210. https://doi.org/10.3390/pr11113210.

Ridichie, A., Ledeţi, A., Sbârcea, L., Rusu, G., Muntean, C., Cîrcioban, D., Peter, F., Ledeţi, I., 2024. Preformulation studies of levonorgestrel. J. Therm. Anal. Calorim. https://doi.org/10.1007/s10973-024-13149-w.

Stauffer, F., Vanhoorne, V., Pilcer, G., Chavez, P.-F., Rome, S., Schubert, M.A., Aerts, L., De Beer, T., 2018. Raw material variability of an active pharmaceutical ingredient and its relevance for processability in secondary continuous pharmaceutical manufacturing. Eur. J. Pharm. Biopharm. 127, 92–103. https://doi.org/10.1016/j.ejpb.2018.02.017.

WHO, 2023. Family Planning/Contraception Methods. World Health Organization.

WHO, 2026. Notes on the Design of Bioequivalence. https://extranet.who.int/prequal/sites/default/files/document_files/BE_Levonorgestrel_May2026.pdf, accessed 23-May-2026.

Xie, B., Liu, Y., Li, X., Yang, P., He, W., 2024. Solubilization techniques used for poorly water-soluble drugs. Acta Pharm. Sin. B 14, 4683–4716. https://doi.org/10.1016/j.apsb.2024.08.027.

Yavuz, B., Chambre, L., Harrington, K., Kluge, J., Valenti, L., Kaplan, D.L., 2020. Silk fibroin microneedle patches for the sustained release of levonorgestrel. ACS Appl. Bio. Mater 3, 5375–5382. https://doi.org/10.1021/acsabm.0c00671.

Zhao, X., Zhang, S., Yang, G., Zhou, Z., Gao, Y., 2020. Exploring trehalose on the release of levonorgestrel from implantable PLGA Microneedles. Polymers 12, 59. https://doi.org/10.3390/polym12010059.

Zulbeari, N., Holm, R., 2024. A systematic investigation of process parameters for small-volume aqueous suspension production by the use of focused ultrasonication. AAPS PharmSciTech 25, 185. https://doi.org/10.1208/s12249-024-02907-6.